Materials Today Bio 25 (2024) 101012

Contents lists available at ScienceDirect

Materials Today Bio

journal homepage: www.journals.elsevier.com/materials-today-bio

Cell sheet formation enhances the therapeutic effects of adipose-derived stromal vascular fraction on urethral stricture

Muxin Li [a], Tianli Yang [b], Jun Zhao [b], Xinghua Ma [a], Yuanyuan Cao [c], Xiaojie Hu [c], Shuli Zhao [a,c,**], Liuhua Zhou [b,*]

[a] General Clinical Research Center, Nanjing First Hospital, China Pharmaceutical University, Nanjing, Jiangsu, China
[b] Department of Urology, Nanjing First Hospital, Nanjing Medical University, Nanjing, Jiangsu, China
[c] General Clinical Research Center, Nanjing First Hospital, Nanjing Medical University, Nanjing, Jiangsu, China

ARTICLE INFO

Keywords:
Stromal vascular fraction
Cell sheet
Urethral stricture
Stem cell therapy
Fibrosis

ABSTRACT

Urethral stricture (US) is a common disease in urology, lacking effective treatment options. Although injecting a stem cells suspension into the affected area has shown therapeutic benefits, challenges such as low retention rate and limited efficacy hinder the clinical application of stem cells. This study evaluates the therapeutic impact and the mechanism of adipose-derived vascular fraction (SVF) combined with cell sheet engineering technique on urethral fibrosis in a rat model of US. The results showed that SVF-cell sheets exhibit positive expression of α-SMA, CD31, CD34, Stro-1, and eNOS. In vivo study showed less collagen deposition, low urethral fibrosis, and minimal tissue alteration in the group receiving cell sheet transplantation. Furthermore, the formation of a three-dimensional (3D) tissue-like structure by the cell sheets enhances the paracrine effect of SVF, facilitates the infiltration of M2 macrophages, and suppresses the TGF-β/Smad2 pathway through HGF secretion, thereby exerting antifibrotic effects. Small animal in vivo imaging demonstrates improved retention of SVF cells at the damaged urethra site with cell sheet application. Our results suggest that SVF combined with cell sheet technology more efficiently inhibits the early stages of urethral fibrosis.

1. Introduction

Urethral stricture (US) is a common urological disorder, predominantly affecting males. Although its pathogenesis remains unclear, the primary pathologic feature is cavernous fibrosis of the urethra, triggered by excess collagen formation following infection or injury [1]. As US progresses, it can lead to urination difficulties, resulting in pain, urinary tract infections (UTIs), and potential renal injury, significantly impairing patients' quality of life. Current treatments involving autologous grafts or flaps from the buccal mucosa and genital skin, while available, are still associated with various complications [2,3]. Recently, tissue engineering has emerged as an alternative approach for urethral reconstruction, utilizing progenitor and stem cells, alongside biomaterials like decellularized tissue matrices and synthetic polymers. However, developing optimal engineered tissue structures for implantation in US treatment remains a significant challenge in urologic research [4].

Adipose tissue offers a promising source of stem cells for tissue engineering and regenerative medicine due to its ready availability and high histocompatibility. The stromal vascular fraction (SVF), a heterogeneous cell population derived from adipose tissue, serves as a rich source of cells for immediate therapeutic application. According to a joint statement by the International Society for Cellular Therapy and the International Federation for Adipose Therapy and Science in 2013, SVF comprises a diverse array of cells including adipose-derived mesenchymal stem cells (ADSCs), endothelial and endothelial progenitor cells, lymphocytes, hematopoietic lineage cells, pericytes, and other components [5]. SVF and ADSCs can similarly affect surrounding cells through paracrine signaling to facilitate a range of biological processes essential for tissue regeneration, including cell differentiation, angiogenesis, immunomodulation, and repair of damaged tissue. The distinctive heterogeneous cellular composition of SVF and its ability to secrete numerous cytokines for synergistic action contribute to the improved therapeutic outcomes observed in animal studies [6–8]. Moreover, the

* Corresponding author. No.68 Changle Road, Nanjing, 210006, Jiangsu, China.
** Corresponding author. No.68 Changle Road, Nanjing, 210006, Jiangsu, China.
E-mail addresses: shulizhao79@njmu.edu.cn (S. Zhao), zlhdyyy@njmu.edu.cn (L. Zhou).

https://doi.org/10.1016/j.mtbio.2024.101012
Received 30 December 2023; Received in revised form 15 February 2024; Accepted 26 February 2024
Available online 29 February 2024
2590-0064/© 2024 The Authors. Published by Elsevier Ltd. This is an open access article under the CC BY-NC-ND license (http://creativecommons.org/licenses/by-nc-nd/4.0/).

simple and rapid preparation process of SVF minimizes contamination risks during cell culture and accelerate tissue repair. SVF cells, derived from freshly isolated autologous adipose tissue, are now applied in a variety of clinical settings, such as osteoarthritis, Crohn's disease, diabetes complications, and aesthetic medicine [9–12], positioning SVF as a straightforward and safe cell group for mitigating damage and promoting functional recovery of different tissues and organs.

While direct injection of suspended cells into the injured area is a common approach that offers some therapeutic benefits, its effects are usually short-lived and low-dose [13,14]. To produce a dense, intact cellular structure that preserves cell-to-cell connections, T. Okano introduced the concept of tissue engineering using cell sheets [15]. The development of cell sheet relies on the temperature-responsive polymer poly (N-isopropylacrylamide) (PIPAAm). Grafting of PIPAAm onto Petri dishes enables the manipulation of cell adhesion and detachment by altering the temperature, thus facilitating the production of cell sheet [16,17]. A significant advantage of cell sheet technology is its ability to provide a three-dimensional (3D) scaffold-free platform for prolonged cell engraftment, survival, and reparative activity. This method has been successfully implemented in various fields. In a clinical study, Ohki et al. transplanted autologous cell sheet derived from oral mucosal epithelial onto the surface of ulcers after endoscopic mucosal debridement in early esophageal cancer, demonstrating the efficacy and safety in promoting wound healing and preventing esophageal stenosis [18]. Additionally, the successful regeneration of mucosa was verified through transplantation of autologous nasal mucosal epithelial cell sheets in treating persistent otitis media [19]. Pluripotent stem cell sheets play a crucial part in alleviating cardiac dysfunction and improving the clinical outcomes of heart failure by forming a vascularized network and delivering sustained therapeutic effects post-transplantation at ischemic sites [20]. Numerous studies have demonstrated that stem cells transplanted via cell-sheet technology exhibit greater transplantation efficiency and longevity in vivo, fulfilling various functions such as tissue reconstruction, anti-inflammatory responses, and vascular regeneration, thereby achieving the desired therapeutic results.

Currently, the regenerative repair of tissues and organs faces a significant challenge due to the lack of suitable sources of stem cells and cell carriers. SVF shows considerable potential as an innovative source of stem cells for tissue regeneration and repair. When combined with cell sheet technology, it may significantly enhance the efficacy of cell therapy and transplantation efficiency. Preclinical evaluation research on stem cells, utilizing cell sheet technology, offers a promising approach to the prevention and treatment of urethral stenosis.

2. Methods

2.1. Animal

The study included 36 male Sprague-Dawley rats, weighing between 220 and 250 g and aging 10 weeks. The rats were housed in a typical environment with controlled humidity and temperature, as well as a 12 h light/dark cycle. Animals were freely offered with food and water. All animal experiments were approved by the Animal Care Committee of Nanjing First Hospital, Nanjing Medical University.

2.2. Cell culture

The human urinary tract epithelial cell line SV-HUC-1 and the mouse monocytic cell line RAW 264.7 were obtained from the cell bank of the Chinese Academy of Science. Ham's F12 medium was used for the culture of SV-HUC-1. To simulate urethral fibrosis in vitro, 5 ng/mL of TGF-β1 (PeproTech, Rocky Hill, NJ, USA) was added into the medium to induce fibrosis of SV-HUC-1. RAW 264.7 was cultured in Dulbecco's modified Eagle medium (DMEM), and exposed to 50 ng/mL of Interferon gamma (IFN-γ, MedChem Express, Monmouth Junction, NJ, USA) and 2 μg/mL of lipopolysaccharide (LPS, Sigma-Aldrich, St. Louis, MO, USA) to induce the M1 phenotype. All media were supplemented with 1% penicillin/streptomycin and 10% fetal bovine serum (FBS, Gibco).

2.3. SVF preparation and flow cytometry

Autologous SVF cells were extracted from epididymal adipose tissue according to our previously reported technique [21]. Briefly, adipose tissue was collected, cut into pieces, and then digested by using 0.075% type I collagenase at 37 °C on a shaker. SVF cell precipitates were collected after multiple centrifugation and washing steps. Cells were stained with fluorescently-labeled antibodies against CD106, VEGFR-2, CD34, CD45, CD90, CD31, and CD4. Flow cytometry was performed using a FACSCaliber (BD Biosciences, San Diego, CA), while FlowJo was used for data analysis. A comprehensive list of antibodies is provided in Supplemental Table S1.

2.4. Cell labeling

According to the instructions, SVF cells were labeled with the lipophilic fluorochrome chloromethyl benzamido dialkyl carbocyanine (CM-DiI; Invitrogen, Carlsbad, CA, USA). In summary, SVF cells were treated with CM-DiI for 5 min at 37 °C, with the concentration of 1 μg CM-DiI per 10^6 cells, followed with incubation for 15 min at 4 °C. At last, the SVF cells were washed, collected, and used for the following experiments.

2.5. Cell culture using temperature-responsive culture dishes

SVF suspensions were inoculated in temperature-responsive dishes (Thermo Fisher Scientific, Nunc Upcell 6, Waltham, MA, USA), and the cells were distributed at 2×10^5 cells/cm^2. When cell adhesion was complete, the culture was continued with 5 ng/mL L-ascorbic acid in fresh medium (Biosharp, Hefei, China). The temperature-sensitive plates were incubated at a lower temperature (25 °C) for an additional 30 min following a 14-day culture period. Then, the cell sheets separated spontaneously.

2.6. Scanning electron microscopy

Cell sheet samples were fixed for 2 h with 2.5% glutaraldehyde, dehydrated by using ethanol of different concentrations (30%, 50%, 70%, 85%, 90%, and 100%), and then dried in a freeze dryer. Finally, the samples were coated with platinum sputtering and examined under scanning electron microscopy.

2.7. Study design

Thirty-six SD rats were randomly divided into four groups: sham-operated group (Sham, n = 6), PBS-treated after US group (US, n = 6), SVF cell suspension-treated after US group (SVF, n = 12), and SVF cell sheet-treated after US group (Cell sheet, n = 12). Among them, the rat urethral stricture model was established in the PBS group, SVF group, and Cell sheet group, respectively. Briefly, a urinary catheter was inserted into the rat after anaesthesia. The penis was incised along the ventral midline until the urethra was exposed, after which human recombinant TGF-β1 (PeproTech) (1 μg/100 μL) was injected into the urethral wall. Five minutes later, four incisions were made in each layer of the penile urethral wall until the catheter was visible. Finally, the catheter was withdrawn, and the incisions were sutured with 5-0 absorbable threads.

2.8. Microultrasound assessment

Tweenty-eight days after surgery, rats underwent micro-ultrasound evaluation for the signs of urethral fibrosis using a Vevo 2100 system.

2.9. Histopathology and immunofluorescent staining (IF)

Urethral tissues were fixed, dehydrated, and embedded. 5 μm slices were cut for staining with hematoxylin, eosin (H&E), and Masson's trichrome. Each slice in all groups were evaluated by pathologists through a standard light microscope (Olympus BX53, Tokyo, Japan). Immunofluorescence staining was performed to analyze the angiogenesis and macrophage infiltration in urothelial tissues. The slices of cell sheet samples and urethral tissues were incubated overnight at 4 °C with primary antibodies including eNOS, α-SMA, Stro-1, CD31, CD34, CD86, CD163, and F4/80. On the second day, slices were stained with Alexa Fluor-conjugated secondary antibody. After DAPI staining for cell nuclei, fluorescence intensity was quantified by ImageJ. A list of the antibodies is provided in Supplemental Table S3.

2.10. Cell tracking and in vivo imaging

SVF cell tracking was carried out by identifying CM-Dil-tagged cells according to our previous protocol [22]. Briefly, urethral tissues were taken at 7, 14, and 28 days after US, frozen in freezing embedding solution (OCT compound), and then serially sectioned at 5 mm intervals. Following nuclear staining with DAPI, red fluorescent-labeled cells were observed under a fluorescence microscope.

After 1, 4, and 17 days of transplantation, rats were given D-luciferin (150 mg/kg of body weight) (Biosynth AG, Staad, Switzerland) by intraperitoneal injection. Five minutes later, the cells were visualized by the PerkinElmer in vivo imaging system IVIS (Xenogen Corp., Hopkinton, MA, USA), which spectrally captured bioluminescence images, and total bioluminescence was analyzed using Living Image software.

2.11. Enzyme-linked immunosorbent assay

Immediately after harvesting cell sheets, the culture mediums of SVF monolayers and SVF cell sheets were replaced with fresh DMEM medium containing 10% FBS, and then the samples were incubated at 37 °C with 5.0% CO_2. After 24 h, the supernatants from all the groups (n = 3) were collected and centrifuged at 2000 × *g* for 20 min to precipitate cell debris and retain the soluble proteins in the supernatants. The concentration of soluble HGF was quantified by using the Rat HGF Quantification Factor ELISA Kit (BYabscience, Nanjing, China), and the absorbance was detected at 450 nm with a microplate reader. HGF concentration in the samples was determined according to the standard curve.

2.12. Reverse transcription-quantitative PCR (RT-PCR) analysis

Total RNA from cultured cells and urethral tissues was extracted using Trizol reagent (Invitrogen), and cDNA was synthesized using Prime Script® RT Master Mix (Vazyme, Nanjing, China). Real-time PCR was performed in triplicate with the SYBR Green PCR kit (Vazyme) on the Biological Systems Q5. The relative expression levels of mRNA were analyzed by the $2^{-\Delta\Delta Ct}$ method. A list of primers used in qRT-PCR is provided in Supplemental Table S2.

2.13. Western blotting

Proteins were extracted from cells and tissues using RIPA buffer (KeyGene Biotech, Nanjing, China) containing protease and phosphatase inhibitors (KeyGene Biotech). The BCA protein assay kit (KeyGene Biotech) was used for the measurement of protein concentrations. Equal amounts of proteins (15 μg/lane) were separated by 10% SDS-PAGE and transferred to the polyvinylidene fluoride membranes (Bio-Rad, Hercules, CA, USA). After being blocked with skim milk for 2 h, the membrane was treated with several primary antibodies for 16 h. Then the membrane was incubated with secondary antibodies for 2 h. Chemiluminescent devices and ECL detection reagents were used to visualize the signals. Antibodies used in western blotting are listed in Supplemental Table S3.

2.14. Statistical analysis

Each experiment was performed in triplicate. The data are expressed as the mean ± standard deviation. The two-sided Student's *t*-test was used for the comparison of two groups, and a parametric or nonparametric ANOVA test was used for multiple-comparison experiments. Statistically significant differences were denoted as follows: $*P < 0.05$; $**P < 0.01$; $***P < 0.001$.

3. Results

3.1. Isolation and identification of SVFs

SVF was isolated from rat epididymal adipose tissue. Flow cytometry analysis showed that both uncultured primary SVF (Fig. 1A, P0) and first-generation SVF (Fig. 1B, P1) consisted of heterogeneous cell populations. They expressed hematopoietic (CD45 [P0 16.5% ± 2.87%; P1 32.6% ± 3.55%] and CD34 [P0 1.3% ± 0.12%; P1 6.94% ± 0.72%]), mesenchymal (CD90 [P0 37.2% ± 3.72%; P1 35,2% ± 3.12%], and CD106 [P0 9.37% ± 9.73%; P1 56.2% ± 4.71%]), endothelial (CD31 [P0 33.6% ± 4.05%; P1 92.6% ± 6.11%] and VEGFR2 [P0 25.9% ± 3.7%; P1 5.92% ± 6.11%]) and T regulatory cells (CD4 [P0 17.6% ± 4.31%; P1 6.51% ± 2.77%]) markers.

Clone formation assay was performed to detect the stemness of SVF. As shown in Fig. 1C, a significant reduction in clonogenic capacity with increased cell passages.

3.2. Construction and characterization of SVF-cell sheet

The SVF-cell sheets were harvested by temperature reduction at 20 °C for 30 min. A large number of spindle-shaped cells with uniform distribution and abundant ECM secretion were observed under inverted phase contrast microscope (Fig. 2A). The detached SVF-cell sheet appeared as a soft white transparent membrane, which macroscopically showed a reduction in diameter and an increase in thickness (Fig. 2B). Hematoxylin and eosin (H&E) staining showed that the SVF-cell sheet could secrete a large amount of ECM and had a 3- or 4-layer cell structure (Fig. 2C). Scanning electron microscopy (SEM) showed that the SVF-cell sheet had a cobblestone-like morphology with a large amount of ECM formed around the SVF cells and tight intercellular connections (Fig. 2D). In addition, immunofluorescence showed that the harvested SVF-cell sheet was positive for CD31, CD34, eNOS, α-SMA, and Stro-1 (Fig. 2E), indicating their potential for differentiation.

3.3. Biodistribution and persistence of SVF in vivo

The enriched ECM structure of the cell sheet layer is essential for improving the survival time and retention of SVF. We labeled SVF with fluorescent dyes and then prepared cell sheets for transplantation into the rat penile area. At 7, 14, and 28 days after surgery, the location of transplanted SVF was detected by fluorescence microscopy. As shown in Fig. 3A, the retention time of SVF-cell sheet was significantly prolonged compared with that of direct SVF injection. A great deal of red labeling of CM-DiI was observed in the SVF-cell sheet group at 28 days, while it was nearly undetectable in the SVF group by 14 days.

In addition, we successfully developed fluorescein-labeled SVF (Luc-SVF). At 1, 4, and 17 days after transplantation of Luc-SVF, photon emission was measured from rat penises after injection of D-luciferin. As shown in Fig. 3B, the transplanted Luc-SVF cell sheets survived longer compared with the directly injected Luc-SVF. Fluorescence intensity in the SVF-cell sheet group was still detectable at 17 days, whereas it significantly diminished in the Luc-SVF group.

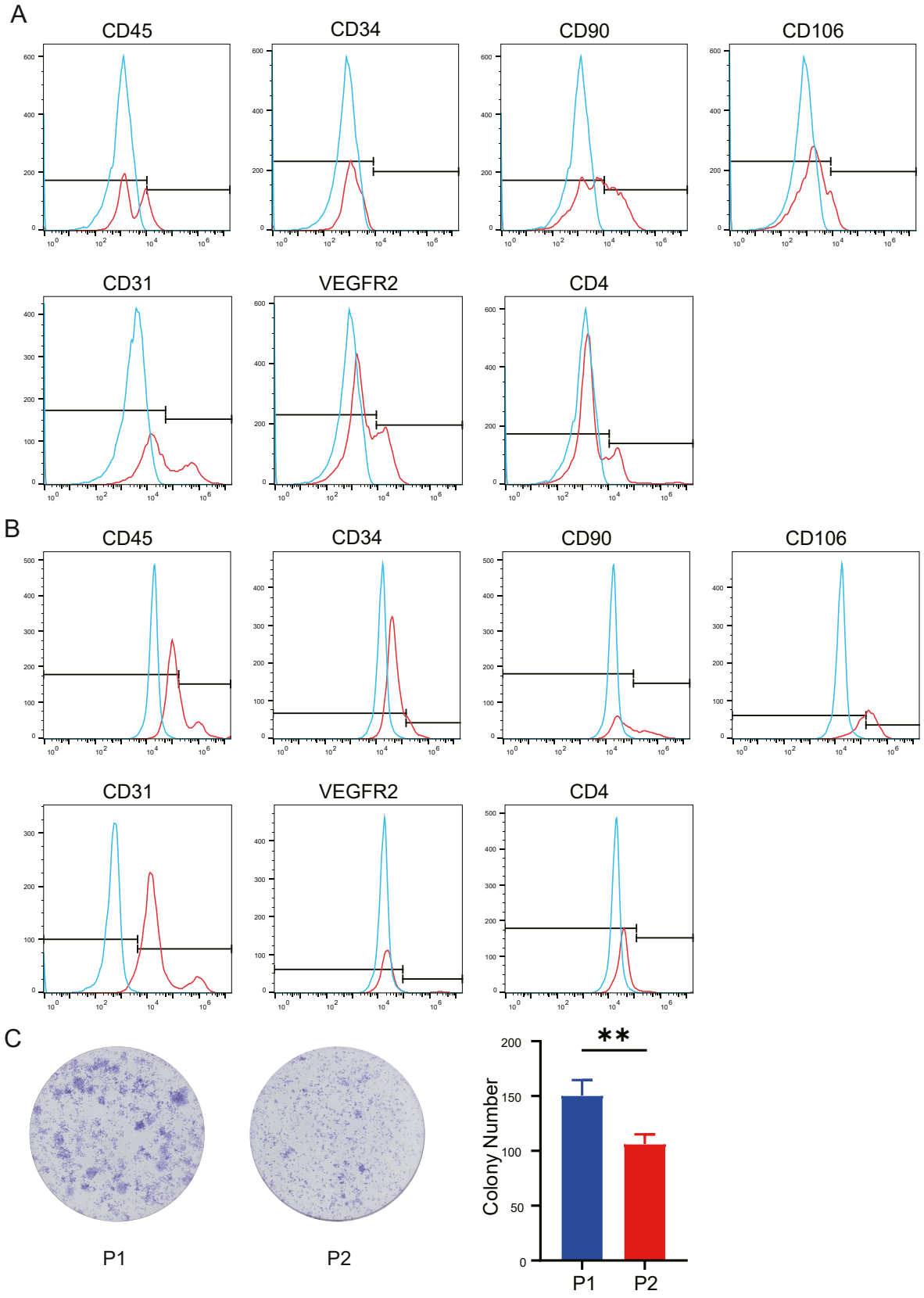

Fig. 1. SVFs identification (A–B) Representative flow cytometry histograms of primary (A, P0) and first-generation (B, P1) adipose-derived stromal vascular fraction (SVF). Results indicated that they express hematopoietic (CD45 and CD34), mesenchymal (CD90 and CD106), endothelial (CD31 and VEGFR2), and T regulatory cell (CD4) markers. The blue lines represent isotype controls. (C) Determination and statistics of colony-forming units (CFU) of first-generation (P1) and second-generation (P2) SVF. (For interpretation of the references to colour in this figure legend, the reader is referred to the Web version of this article.)

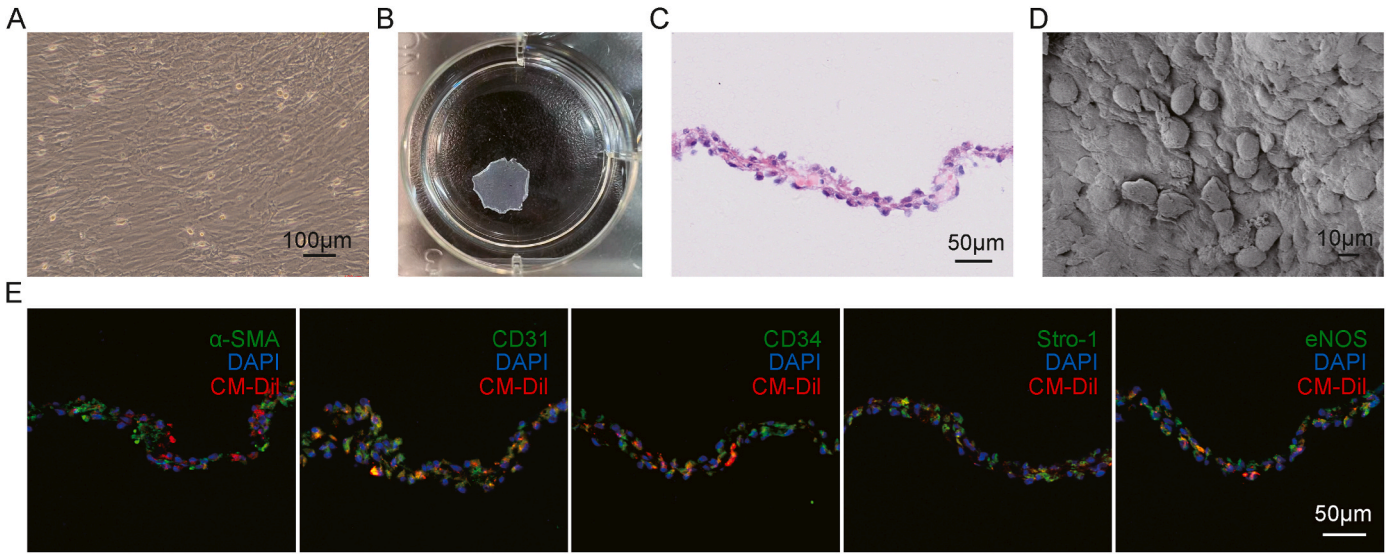

Fig. 2. Cell sheet formation and identification. (A) A SVF-cell sheet was observed under an inverted microscope (scale bar: 100 μm). (B) SVF-cell sheet formation after 14 days of continuous culture. (C) H-E staining results of the SVF-cell sheet. The cell sheet consists of 3- or 4-layers of cells (scale bar: 50 μm). (D) SEM image of the SVF-cell sheet (scale bar: 10 μm). (E) The result of immunofluorescence showed positive staining of α-SMA, CD31, CD34, Stro-1, and eNOS in the SVF-cell sheet (scale bar: 50 μm).

3.4. SVF-cell sheet alleviates urethral fibrosis and promotes structural repair

To verify the therapeutic effect of SVF, a rat model of urethral stricture was used to compare the reparative outcomes of cell suspension and cell sheet treatments. The urethral repair process was evaluated by micro-ultrasound at 28 days after surgery. Micro-ultrasound evaluation indicated that compared to the sham group, the US group exhibited hyperechoic urethral walls and constriction of the urethral lumen. Conversely, the SVF and the Cell sheet groups showed less noticeable urethral strictures and hyperechoic tissue (Fig. 4A).

Histologic testing was performed at 28 days postoperatively to further evaluate the urethral repair from a microscopic perspective. H&E and Masson staining revealed that urethral specimens from the US group showed sparse smooth muscle and pronounced submucosal fibrosis. SVF treatment attenuated this process. Notably, the urethral cavernous body of the Cell sheet group showed minimal submucosal fibrosis and tissue alteration (Fig. 4B, C).

To elucidate the structural remodeling and repair facilitated by the SVF-cell sheet, we used immunofluorescence staining to analyze the epithelialization of AE1/AE3. In the US group, thin and discontinuous epithelial cells were observed at the repair site after 28 days. In contrast, in both the SVF and Cell sheet groups, continuous epithelial cells fully covered the defect site, contributing significantly to urethral defect repair (Fig. 4D).

3.5. SVF-cell sheet reduces collagen expression and promotes angiogenesis

TGF-β/Smad signaling pathway plays a crucial role in fibrosis development, and excessive collagen deposition after injury is key feature of urethral fibrosis. To investigate the role and mechanism of SVF-cell sheet attenuating urethral fibrosis, expression level of collagen I, collagen III, and TGF-β/Smad signaling pathway protein in rat urethral tissues was detected by western blotting at 28 days after surgery. Fig. 5A, B showed significantly increased expression of collagen I and III in the US group, indicating collagen deposition occurred in the US urethra. Phospho-Smad2 protein expression was reduced after SVF-cell sheet transplantation, albeit modestly, suggesting the SVF-cell sheet might hinder urothelial tissue fibrosis by targeting the TGF-β/Smad2 pathway. Moreover, the SVF-cell sheet significantly reversed fibrosis and collagen deposition in the urethral tissues, which indicates that SVF-cell sheet has higher therapeutic efficacy than directly injected SVF cell. The gene expression of COL1A1, FN, and CTGF was detected by qRT-PCR. CTGF is induced by TGF-β and is considered to be a downstream mediator of TGF-β action on fibroblasts. Results showed that SVF-cell sheet further suppressed US-induced COL1A1, FN, and CTGF expression. Additionally, since T-helper type 2 responses support selective activation of macrophages, we assessed the Gata3/T-bet ratio of gene expression, which was higher in the Cell sheet group, suggesting a transformation of T-cells toward Th2 differentiation (Fig. 5C).

In addition, the formation of neovascular networks was examined by staining the endothelium markers with CD34 and CD31. Immunofluorescence analysis showed a significant increase in vessel density at 28 days after SVF-cell sheet transplantation (Fig. 5D, E). In addition, protein expression of angiogenesis-related proteins, such as VEGFA and bFGF, was upregulated after SVF treatment, and was further upregulated by the application of cell sheet technology (Fig. 5A–B).

3.6. SVF-cell sheet alleviates urethral fibrosis associated with macrophage phenotype

The formation of urethral tissue fibrosis involves a complex inflammatory response process, in which macrophage infiltration plays an important role. CD86 and CD163 were used as markers for M1 and M2 macrophages, respectively. Tissue immunofluorescence staining revealed elevated CD86 expression in the US group, which may be related to the injury-induced immune response. In contrast, SVF-cell sheet treatment markedly reduced CD86 expression while enhancing CD163 expression (Fig. 6A–C). This suggests that SVF-cell sheet implantation attracted macrophages to the damaged site and prompted their polarization from the M1 to the M2 phenotype, thereby fostering an anti-inflammatory microenvironment. In addition, qRT-PCR analysis confirmed that the expression patterns of Arg1 and Nos2 in the tissues of each group were consistent with the immunofluorescence findings (Fig. 6D).

To further elucidate these findings and explore underlying mechanisms, an in vitro system was established. In this system, SVF cells or SVF cell sheets were co-cultured with LPS/IFN-γ-stimulated RAW264.7. qRT-PCR demonstrated that SVF cell sheets significantly reduced the gene expression of iNOS, IL-1β, and CXCL-10 (M1 markers) and increased the

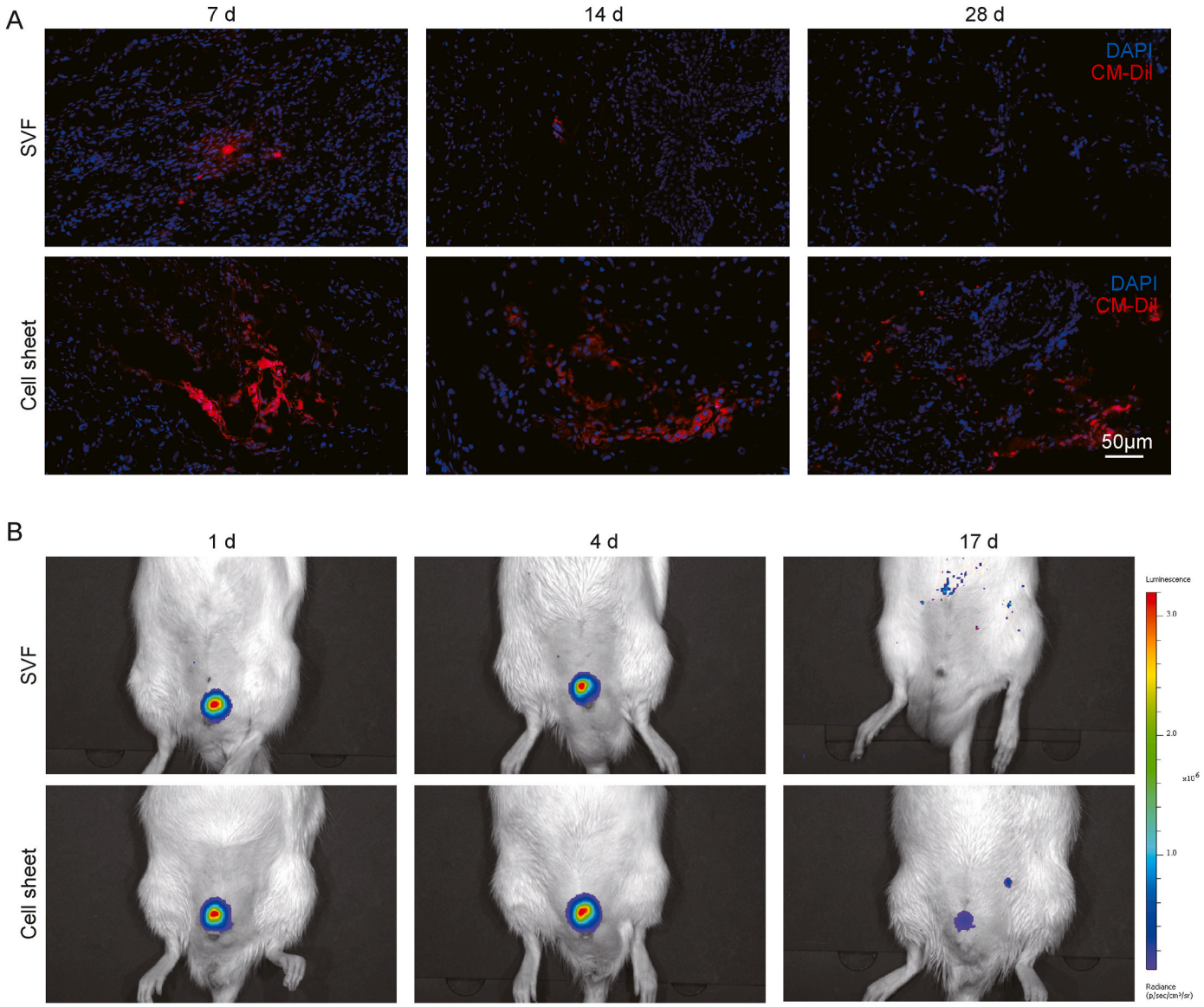

Fig. 3. In vivo tracing and cellular localization of transplanted SVF cells. (A) Cell tracking of CM-Dil-labeled cells in penile urethral tissues from SVF group and Cell sheet group at 7, 14, and 28 days after US (scale bar: 50 μm). (B) Representative images of luciferase signals in the rats were indicated after transplantation of SVF suspension cells or SVF-cell sheets for 1, 4, and 17 days.

gene expression of Arg-1, CD163, and IL-10 (M2 markers) in RAW264.7 (Fig. 6E). Therefore, SVF-cell sheet may mitigate macrophage infiltration and promote macrophage polarization from the M1 to M2 phenotype via paracrine effects, potentially augmenting early urethral stricture treatment.

3.7. SVF alleviated TGF-β-induced fibrosis in vitro

An in vitro uroepithelial fibrosis cell model was established by stimulating SV-HUC-1 with 5 ng/mL TGF-β1. Western blot and qRT-PCR results indicated that the protein and gene expression levels of Collagen I, Collagen III, and Fibronectin were increased by TGF-β1 stimulation. And co-culture with SVF cells partially reversed this trend (Fig. 7A–C).

3.8. 3D cell sheet showed increased expression of pro-regenerative cytokine genes

After the SVF cell sheets were detached, the incubation was continued for 24 h. qRT-PCR results showed that the expression of β-catenin and connexin43, the cell junction communication-related proteins, was significantly increased in the 3D-cell sheet group compared to the 2D-SVF group (Fig. 7D). Additionally, gene expression of vascular endothelial growth factor (VEGF), hepatocyte growth factor (HGF), and anti-inflammatory factor interleukin-10 (IL-10) were upregulated, whereas fibroblast growth factor (FGF) gene expression was downregulated in the 3D-cell sheet group (Fig. 7E). These findings suggest that the genes associated with the tissue-like microenvironment are up-regulated in the SVF-cell sheet, which facilitates the secretion of pro-regenerative cytokines.

3.9. SVF reverses TGF-β-induced fibrosis by HGF released through paracrine effects

To further investigate the paracrine role of the SVF-cell sheet, we detected the HGF concentration in the supernatants of SVF cells and SVF-cell sheet with an ELISA kit. The results showed that SVF-cell sheet secreted more HGF (Fig. 7F). Similarly, ELISA results of rat urethral tissue homogenate supernatants from each group showed higher level of

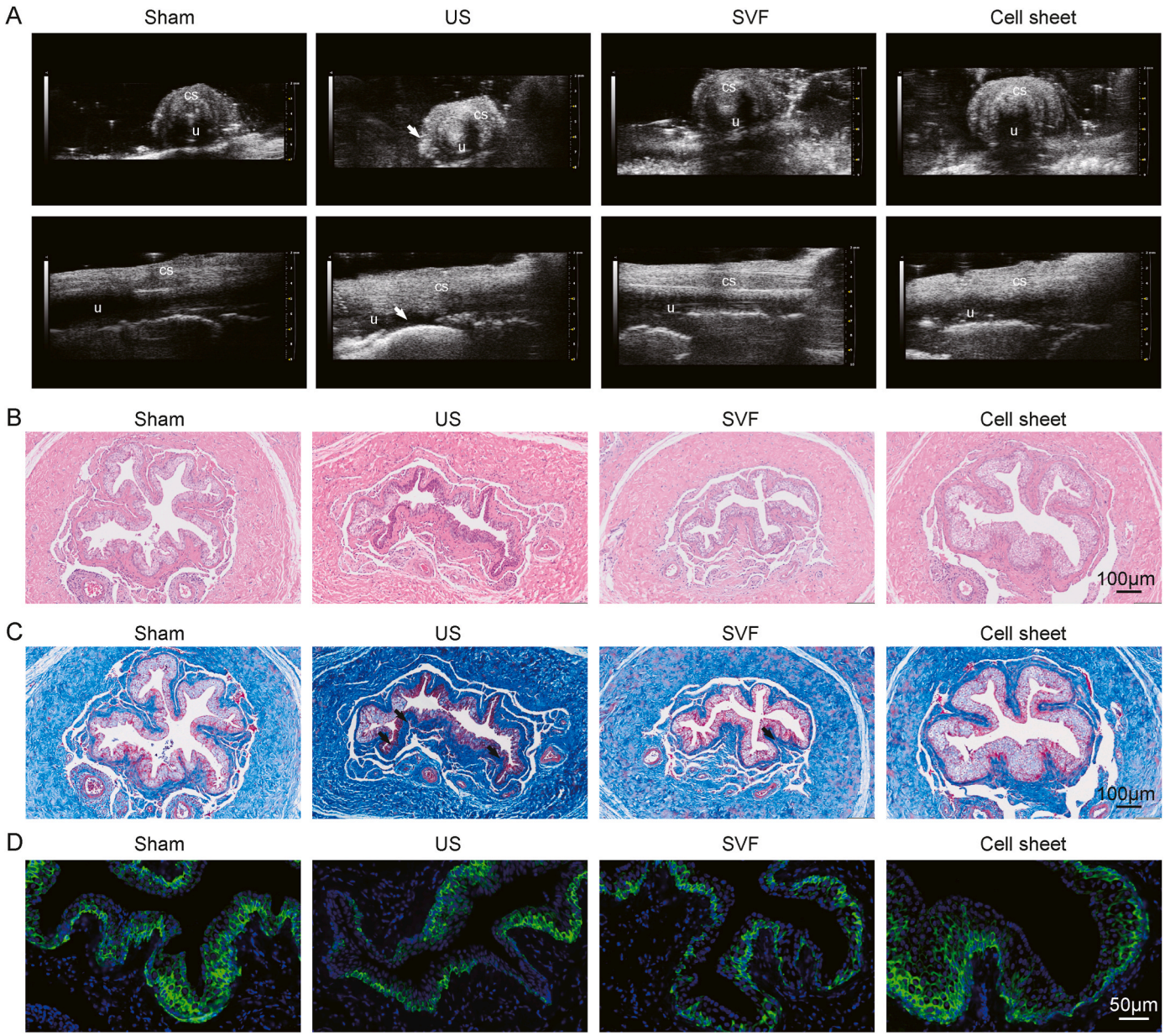

Fig. 4. Transplanted SVF cell sheets alleviate the progression of urethral fibrosis and promote structural repair. (A) Representative micro-ultrasound images of penile urethras in sham, US, SVF, and Cell sheet groups at 28 days after surgery. The arrows indicate the location of hyperechoic tissue and the narrowing of the urethral lumen. CS corpus cavernosum, U urethral lumen. (B–C) Representative microscopic results of hematoxylin and eosin (H&E) and Masson's trichrome staining of urethral tissue in sham, US, SVF, and Cell sheet groups at 28 days postoperatively (scale bar: 100 μm). US group urethral tissues showed densely arranged collagen bundles and sparse smooth muscle. The SVF and Cell sheet groups tissues showed mild submucosal fibrosis and less tissue alteration. Arrows indicate sites of collagen deposition. (D) Immunofluorescence analysis of AE1/AE3 in the repair site urethra (scale bar: 50 μm).

HGF in the Cell sheet group, and qRT-PCR results were consistent with them (Fig. 7G, H).

Western blot and qRT-PCR results showed that the activation of the TGF-β-mediated fibrotic pathway and consequent fibrosis could be prevented by the treatment of recombinant human HGF in an in vitro urethral epithelial cell fibrosis model (Fig. 8A–C). Furthermore, co-culture of HGF-neutralized SVF with TGF-β-treated SV-HUC-1 showed that neutralizing HGF reversed the up-regulation of Fibronectin, collagen III, and p-Smad2 (Fig. 8D–F). Therefore, we conclude that HGF secreted by SVF impedes the TGF-β-mediated activation of the fibrotic pathway and subsequent collagen deposition.

4. Discussion

In a previous study [23], we established a reproducible US animal model and demonstrated that SVF suspensions could mitigate early urethral fibrosis, restoring urethral structure and function [14]. In this work, we first demonstrated that employing an SVF scaffold-free cell sheet in rats with early urethral stricture effectively delays urethral fibrosis formation and the associated tissue injury process. This approach compensates for the technical challenges of direct cell suspension injection, improves cell retention rate, and simplifies the surgical process. Next, we further explored the intrinsic mechanism of the SVF-cell sheet for urethral stricture treatment. We found that SVF-cell sheet can promote the polarization of macrophages from M1 to M2, both in vivo and in vitro. The 3D cell sheet structure could induce SVF to

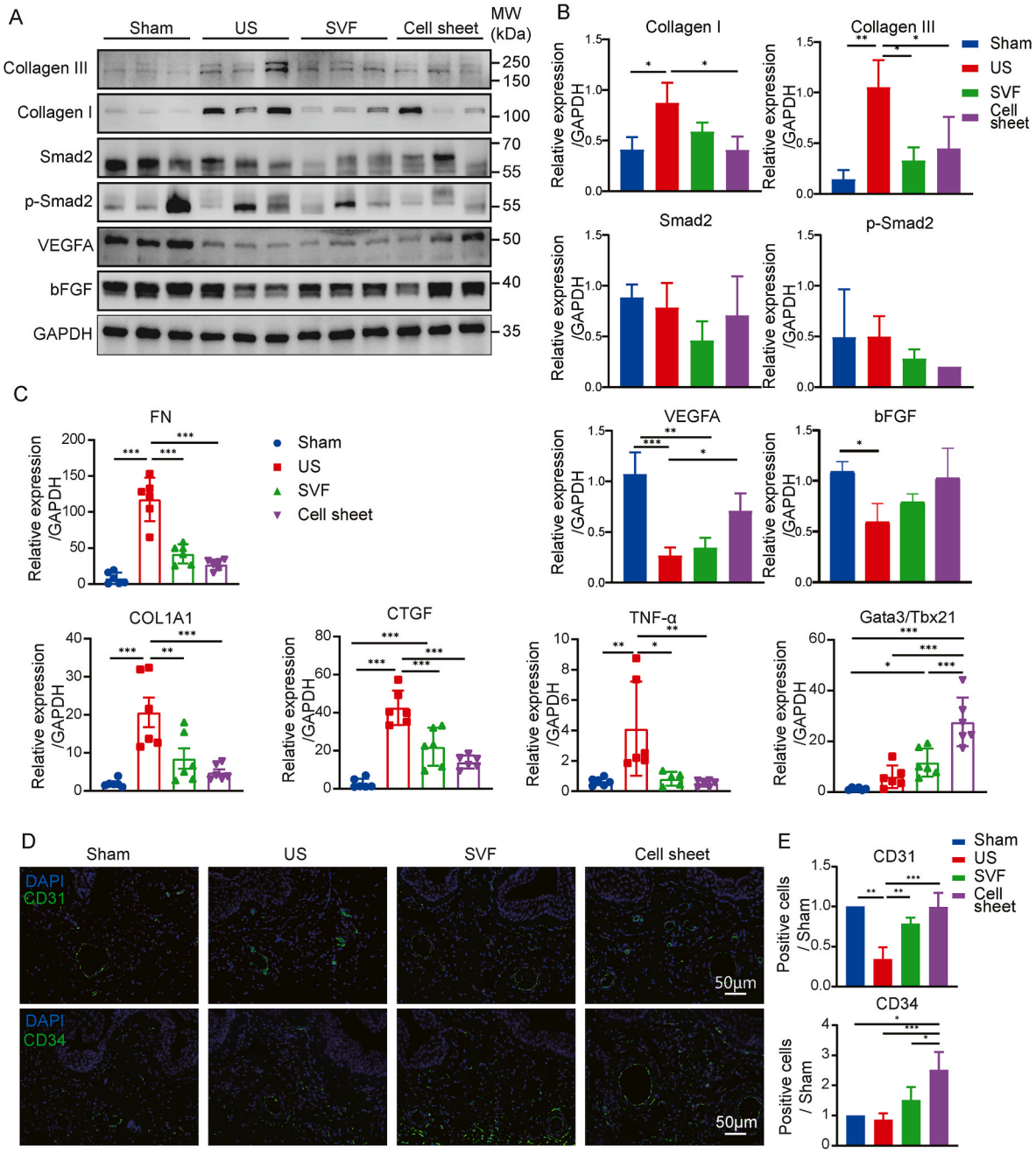

Fig. 5. Transplanted SVF-cell sheet reduces collagen expression and promotes angiogenesis in urethral stricture rats. (A–B) At 28 days after surgery, the expression of Collagen III, Collagen I, Smad2, Phospho-Smad2 (p-Smad2), VEGFA, and bFGF proteins in urethral tissues of Sham, US, SVF, and Cell sheet group was measured by western blot. Quantification was performed using the relative abundance data of the target proteins to GAPDH. (C) Gene expression of FN1, COL3A1, bFGF, CTGF, TNF-α, Gata3, and Txb21 in urethral tissues was measured by real-time PCR in Sham, US, SVF, and Cell sheet groups at 28 days after surgery. (D) Immunofluorescence staining of CD31 and CD34 expression in urethral tissues of Sham, US, SVF, and Cell sheet groups 28 days postoperatively. (scale bar: 50 μm). (E) Quantitative expression levels of CD31 and CD34 in the urethral after different treatments. Data are shown as mean ± SD.*$P < 0.05$, **$P < 0.01$, ***$P < 0.001$.

secrete more repair-related paracrine factors and contribute to more effective therapeutic outcomes.

3D cell sheet tissues can be prepared by cultivating standard 2D adherent cells on temperature-responsive culture dishes coated with PIPAAm [15]. The surface properties of PIPAAm change with the environmental temperature. PIPAAm has hydrophobic qualities at 37 °C, allowing cell growth in the culture dish at normal confluence and inducing extracellular matrix (ECM) deposition to form adhesive interactions among neighboring cells. PIPAAm become hydrophilic when the ambient temperature falls below 20 °C, facilitating cell sheet detachment while retaining ECM, cell adhesion proteins, and intercellular interactions [24,25]. Along with the separation of cell sheets from temperature-responsive dishes, the transition from 2D to 3D structures involves actin skeleton reorganizations, a shift in cell shape from elongated to round, and morphological changes that are visible at the macroscale [26]. One study that created 3D culture platforms using MSC sheet layers discovered that 3D tissue-like microenvironments supported MSC potency by supporting both physical (cell shape and spatial arrangement) and chemical (cellular interactions and expression of binding proteins) effects [27]. Our study revealed that the harvested cell sheets spontaneously contracted with morphological manifestation of diameter reduction and thickness increase. Scanning electron

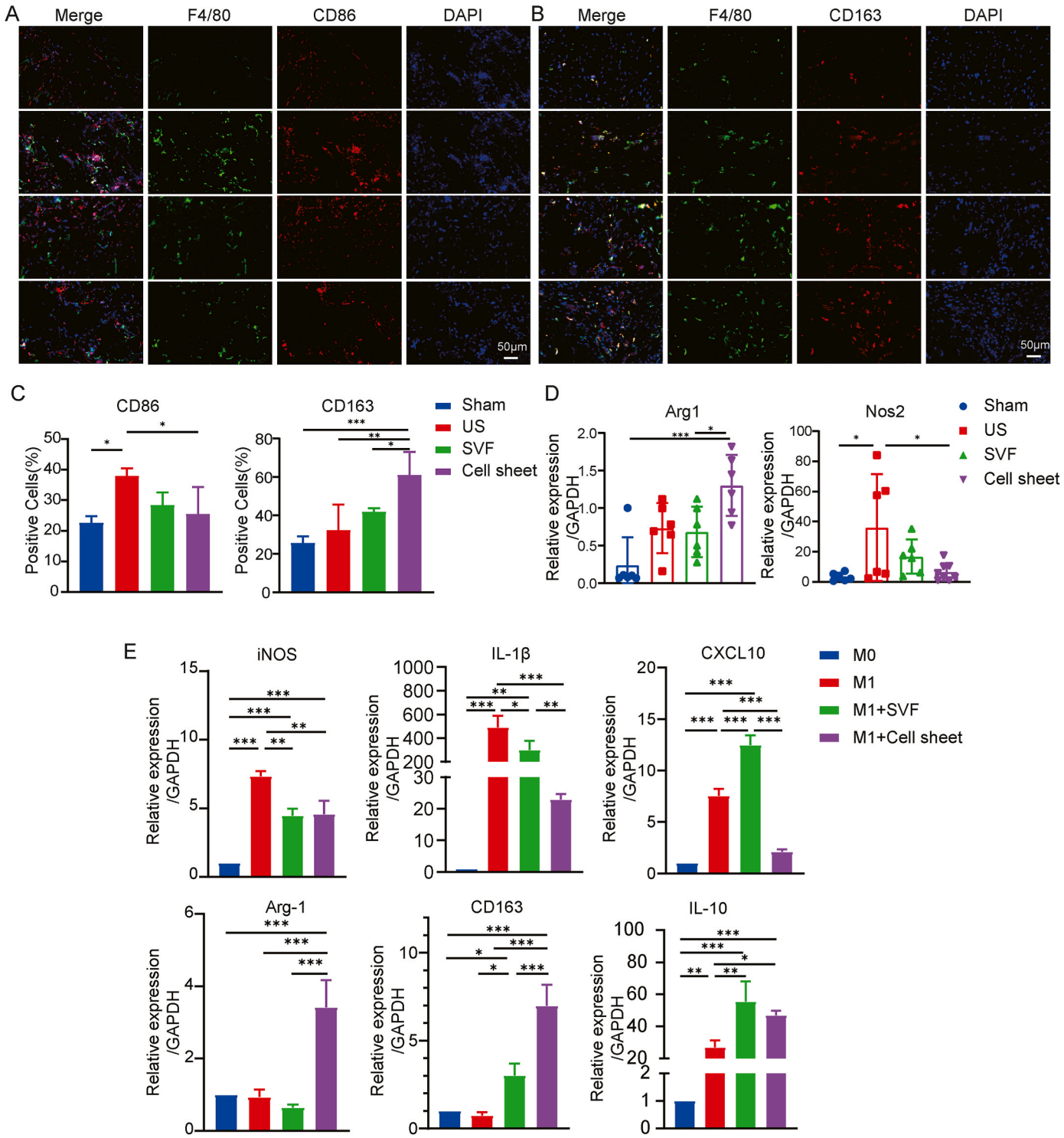

Fig. 6. SVF-cell sheet alleviates urethral fibrosis, which may be related to changes in the phenotypic distribution of periurethral macrophages. (A–B) Immunofluorescence staining of F4/80, CD86, and CD163 in urethral sections from Sham, US, SVF, and Cell sheet groups at 28 days after surgery (scale bar: 50 μm). (C) Semi-quantitative statistics of $CD86^{-}$and CD206-positive cells. (D) Gene expression of Arg1 and Nos2 in urethral tissues was measured by real-time PCR in Sham, US, SVF, and Cell sheet groups 28 days after surgery. (E) SVF cells or SVF-cell sheets were co-cultured with LPS/IFN-γ-treated M1 macrophages, and RT-qPCR was performed to measure M1 macrophage markers and M2 macrophage markers at the mRNA level. Data are shown as mean ± SD.*$P < 0.05$, **$P < 0.01$, ***$P < 0.001$.

microscope revealed a dense structure. In comparison to 2D-SVF cultured in monolayer, the expression of β-catenin and connexin 43 was significantly up-regulated in 3D-cell sheets. β-catenin, part of the adhesion connexin complex, and connexin 43, a gap junction protein, are crucial for cell adhesion and intracytoplasmic signaling [28]. Our findings suggest that the creation of a three-dimensional microenvironment enhances cellular interactions and connectivity, both among cells and between cells and the surrounding matrix. Furthermore, cytokines such as VEGF, IL-10, and the paracrine cytokines HGF and FGF play a critical role in directly regulating tissue regeneration and repair. These cytokines are especially vital for reducing tissue fibrosis, promoting angiogenesis, and suppressing inflammation [29–31]. The

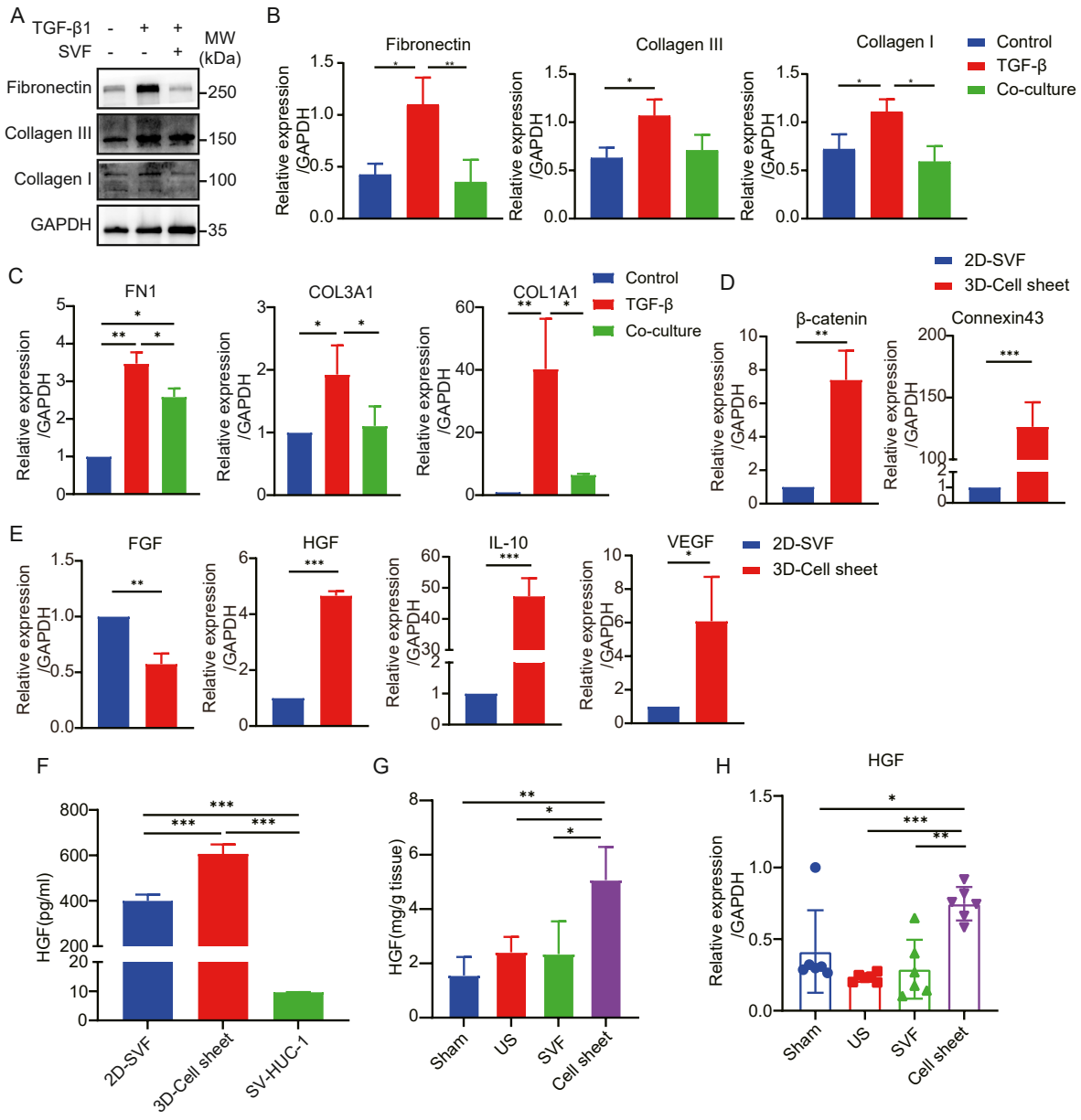

Fig. 7. TGF-β induced in vitro fibrosis model and three-dimensional cell sheet tissue-like structures promote enhanced expression of pro-regenerative cytokine genes, especially HGF. (A–C) The SV-HUC-1 human urinary tract epithelial cell line was treated with TGF-β1 at 5 ng/mL and constructed the co-culture system with SVF. The expression levels of Fibronectin, Collagen I and Collagen III were measured by western blot and qRT-PCR. (D) qRT-PCR results showed that gene expression of interaction-related proteins, including β-catenin (cell-cell interaction) and Connexin 43 (gap junction), was increased in the 3D-cell sheet group compared with the 2D-SVF group. (E) Quantitative gene expression of the pro-regenerative cytokines VEGF, HGF, and IL-10 was also increased, and bFGF gene expression was decreased in the 3D-cell sheet group. (F) The supernatants of 3D-SVF cell sheets and 2D-cultured SVF cells were taken and subjected to ELISA, which showed that 3D-SVF cell sheets secreted higher levels of HGF. (G) 28 days after transplantation of SVF-cell sheets, the supernatant of tissue homogenate from the transplanted area was taken for ELISA, and the results showed that the SVF-cell sheet group continuously secreted HGF. (H) Gene expression of HGF in urethral tissues was measured by real-time PCR in Sham, US, SVF, and Cell sheet groups 28 days after surgery. Data are shown as mean ± SD.*$P < 0.05$, **$P < 0.01$, ***$P < 0.001$.

preservation of a tissue-like microenvironment within the cell sheet was associated with a marked increase in the levels of VEGF, HGF, and IL-10. This three-dimensional architecture significantly boosts SVF's ability to secrete cytokines. Collectively, these results imply that 3D cell sheet structures can improve the therapeutic efficacy of SVF.

By stimulating SVHUC-1 with TGF-β, we created an in vitro urethral epithelial cell fibrosis model to mimic in vivo urethral stricture and enhance our understanding of the anti-fibrotic mechanism of SVF. When cells express the cognate receptor HGFR/c-Met, HGF, a multipotent growth factor, induces anti-inflammatory and anti-fibrotic effects [32]. HGF employs various methods to interfere with Smad signaling. In diabetic hepatic fibrotic mice, it has been demonstrated that co-administration of ADSCs and HGF increases the antifibrotic effects, indicating the potential to downregulate the TGF-β/Smad fibrotic pathway and reduce the expression of fibrotic markers [33]. Injecting anti-HGF antibodies into rats or mice with chronic kidney disease exacerbates the progression of tubulointerstitial fibrosis. Additionally, exogenous HGF inhibits TGF-β expression and halts the progression of renal fibrosis in several experimental models of chronic kidney disease [34]. Our research revealed that 3D cell sheets secreted higher amounts of HGF. Additionally, we discovered that the TGF-β-Smad2 pathway could be prevented in the in vitro urothelial fibrosis model by adding recombinant HGF, which led to a decrease in mRNA and protein expression of Collagen III and FN. In addition, HGF partially mediates

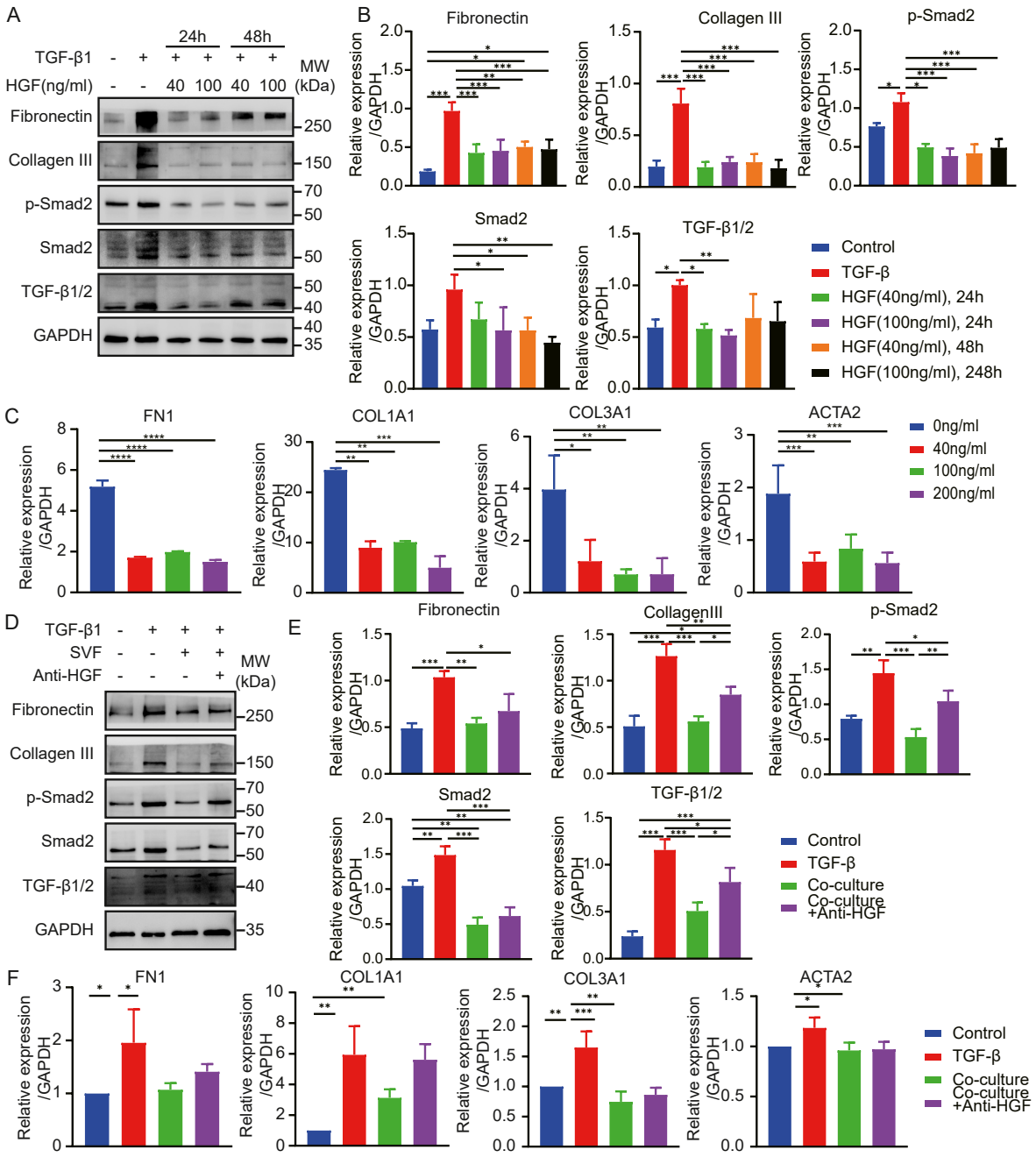

Fig. 8. SVF reverses TGF-β-induced fibrosis by HGF released through paracrine effects. (A–B) Recombinant HGF at different concentrations and treatment times was added to the in vitro fibrosis model. Protein expression levels of Fibronectin, Collagen III, p-Smad2, Smad2, and TGF-β1/2 were measured and quantified by Western blot. (C) FN, COL1A1, COL3A1, and ACTA2 gene expression levels were determined by qRT-PCR. (D) SVF cells treated with 1 μg/mL HGF-neutralizing antibody were co-cultured with TGF-β-stimulated SV-HUC-1. Protein expression levels of Fibronectin, Collagen III, p-Smad2, Smad2, and TGF-β1/2 were measured and quantified by Western blot. (E) FN, COL1A1, COL3A1, and ACTA2 gene expression levels were determined by qRT-PCR. Data are shown as mean ± SD.*$P < 0.05$, **$P < 0.01$, ***$P < 0.001$.

the reparative effects of SVF on urethral fibrosis, as effects are somewhat blocked by the HGF-neutralizing antibody. Since SVF and SVHUC-1 are grown in a physically isolated co-culture environment, it can be concluded that SVF-secreted HGF acts in a paracrine manner. This finding suggests a mechanism by which SVF-secreted HGF promotes the recovery of urothelial fibrosis.

Macrophages are known for their high plasticity. They exhibit a variety of phenotypes and functions (polarization) in response to varying environmental conditions and participate in all stages of tissue repair. After an injury, M1 macrophages play a crucial role in initiating inflammatory response, while M2 macrophages participate in both the healing of injured tissue and the reduction of inflammation. M2 macrophages have been linked to the progression of numerous fibrotic diseases according to several studies [35,36]. Our present study showed that, four weeks after US, the rat exhibited significant deposition of extracellular matrix components, including Collagen I and Collagen III, accompanied by M2 macrophage infiltration. SVF cells isolated from adipose tissue contain monocytes or macrophages that express IL-1 and IL-10 at high levels, contributing to anti-inflammatory effects [37]. In addition, SVF cells have the capacity to selectively regenerate damaged tissue and modulate functions directly or indirectly [38]. Immunofluorescence results suggest that SVF regulates macrophage polarization

during the inflammatory phase of healing process, which in turn affects both inflammation and tissue regeneration. Previous studies have shown that MSCs in SVF induce macrophage polarization towards the M2 phenotype through the secretion of growth factors and cytokines such as IL-4, IL-10, and TGF-β [39]. In our study, SVF-cell sheet treatment significantly increased M2 macrophage infiltration in urothelial tissue. RAW264.7 transformed into M1-type macrophages by LPS/IFN-γ stimulation and SVF treatment showed typical down-regulation of M1 markers iNOS, IL-1β, and CXCL10 and up-regulation of M2 markers CD163, Arg-1, and IL-10, aligning with our in vitro findings. However, the mechanisms of macrophage activation are poorly understood, and the question of how SVF, as a heterogeneous population, induces macrophage polarization requires further investigation.

5. Conclusions

In this work, we developed 3D structured SVF-cell sheet, which led to an innovative therapy for urethral strictures. This structure offered a three-dimensional culture environment that preserved cellular bioactivity, increased the paracrine effects of cytokines, and minimized their degradation. Significantly, the anti-fibrotic function of SVF was improved when combined with cell sheet technology, offering significant therapeutic advantages in the rat model of urethral fibrosis. In addition, our study demonstrated that SVF-cell sheet expressed a higher level of VEGF and HGF, as well as suppressed inflammation and attenuated fibrosis by promoting polarization of M1 macrophages toward the M2 phenotype and modulating the TGF-β/Smad2 signaling pathway in a rat urethral stricture model induced by TGF-β. These results indicated clinical potential of cell therapy combined with cell sheet technology. Further investigation is necessary to elucidate how each cell type contributes to urethral stricture therapy, due to the heterogeneity of the SVF-cell sheet.

Statement of significance

Urethral stricture is one of the common diseases in urology, and urethral spongy fibrosis caused by collagen overproduction after infection or injury affects the life quality of patients. We designed SVF-cell sheet by stromal vascular fraction (SVF) combined with scaffold-free cell sheet technology, validated its characterization in vitro, and found that SVF-cell sheet showed higher efficacy in rats with urethral stenosis. These evidences demonstrate the promise of SVF-cell sheet as a new treatment for urethral stricture in the clinic.

CRediT authorship contribution statement

Muxin Li: Writing – original draft, Investigation, Conceptualization. **Tianli Yang:** Investigation. **Jun Zhao:** Investigation. **Xinghua Ma:** Formal analysis. **Yuanyuan Cao:** Formal analysis. **Xiaojie Hu:** Investigation. **Shuli Zhao:** Funding acquisition, Conceptualization. **Liuhua Zhou:** Writing – review & editing, Writing – original draft, Funding acquisition, Conceptualization.

Declaration of competing interest

The authors declare that they have no known competing financial interests or personal relationships that could have appeared to influence the work reported in this paper.

Data availability

Data will be made available on request.

Acknowledgments

This work was supported by Jiangsu Provincial Medical Youth Talent (QNRC2016071), Nanjing Medical Science and Technology Development Project, China (JQX17007, YKK20103), and National Natural Science Foundation of China (grant number: 82173205)

Appendix A. Supplementary data

Supplementary data to this article can be found online at https://doi.org/10.1016/j.mtbio.2024.101012.

References

[1] A.R. Mundy, D.E. Andrich, Urethral strictures, BJU Int. 107 (2011) 6–26.
[2] W. Verla, W. Oosterlinck, A.-F. Spinoit, M. Waterloos, A comprehensive review emphasizing anatomy, etiology, diagnosis, and treatment of male urethral stricture disease, BioMed Res. Int. 2019 (2019) 1–20.
[3] A. Raya-Rivera, D.R. Esquiliano, J.J. Yoo, E. Lopez-Bayghen, S. Soker, A. Atala, Tissue-engineered autologous urethras for patients who need reconstruction: an observational study, Lancet 377 (2011) 1175–1182.
[4] Z. Rashidbenam, M.H. Jasman, P. Hafez, G.H. Tan, E.H. Goh, X.I. Fam, C.C.K. Ho, Z.M. Zainuddin, R. Rajan, F.M. Nor, M.A. Shuhaili, N.R. Kosai, F.H. Imran, M. H. Ng, Overview of urethral reconstruction by tissue engineering: current strategies, clinical status and future direction, Tissue Eng Regen Med 16 (2019) 365–384.
[5] P. Bourin, B.A. Bunnell, L. Casteilla, M. Dominici, A.J. Katz, K.L. March, H. Redl, J. P. Rubin, K. Yoshimura, J.M. Gimble, Stromal cells from the adipose tissue-derived stromal vascular fraction and culture expanded adipose tissue-derived stromal/stem cells: a joint statement of the International Federation for Adipose Therapeutics and Science (IFATS) and the International Society for Cellular Therapy (ISCT), Cytotherapy 15 (2013) 641–648.
[6] L. Charles-de-Sá, N.F. Gontijo-de-Amorim, C. Maeda Takiya, R. Borojevic, D. Benati, P. Bernardi, A. Sbarbati, G. Rigotti, Antiaging treatment of the facial skin by fat graft and adipose-derived stem cells, Plast. Reconstr. Surg. 135 (2015) 999–1009.
[7] D. You, M.J. Jang, B.H. Kim, G. Song, C. Lee, N. Suh, I.G. Jeong, T.Y. Ahn, C.-S. Kim, Comparative study of autologous stromal vascular fraction and adipose-derived stem cells for erectile function recovery in a rat model of cavernous nerve injury, Stem Cells Transl. Med. 4 (2015) 351–358.
[8] J.A. Semon, X. Zhang, A.C. Pandey, S.M. Alandete, C. Maness, S. Zhang, B. A. Scruggs, A.L. Strong, S.A. Sharkey, M.M. Beuttler, J.M. Gimble, B.A. Bunnell, Administration of murine stromal vascular fraction ameliorates chronic experimental autoimmune encephalomyelitis, Stem Cells Transl. Med. 2 (2013) 789–796.
[9] M. Moustaki, O. Papadopoulos, C. Verikokos, D. Karypidis, D. Masud, A. Kostakis, F. Papastefanaki, M.G. Roubelakis, D. Perrea, Application of adipose-derived stromal cells in fat grafting: basic science and literature review, Exp. Ther. Med. 14 (2017) 2415–2423.
[10] J. Hedhli, C.J. Konopka, S. Schuh, H. Bouvin, J.A. Cole, H.D. Huntsman, K. A. Kilian, I.T. Dobrucki, M.D. Boppart, L.W. Dobrucki, Multimodal assessment of mesenchymal stem cell therapy for diabetic vascular complications, Theranostics 7 (2017) 3876–3888.
[11] G.W. Dryden, E. Boland, V. Yajnik, S. Williams, Comparison of stromal vascular fraction with or without a novel bioscaffold to fibrin glue in a porcine model of mechanically induced anorectal fistula: inflammatory bowel diseases 23 (2017) 1962–1971.
[12] J. Pak, Regeneration of human bones in hip osteonecrosis and human cartilage in knee osteoarthritis with autologous adipose-tissue-derived stem cells: a case series, J. Med. Case Rep. 5 (2011) 296.
[13] P. Sharma, A. Kumar, A.D. Dey, T. Behl, S. Chadha, Stem cells and growth factors-based delivery approaches for chronic wound repair and regeneration: a promise to heal from within, Life Sci. 268 (2021) 118932.
[14] X. Chen, M. Lu, N. Ma, G. Yin, C. Cui, S. Zhao, Dynamic tracking of injected mesenchymal stem cells after myocardial infarction in rats: a serial 7T MRI study, Stem Cell. Int. 2016 (2016) 1–10.
[15] N. Yamada, T. Okano, H. Sakai, F. Karikusa, Y. Sawasaki, Y. Sakurai, Thermo-responsive polymeric surfaces; control of attachment and detachment of cultured cells, Makromol. Chem., Rapid Commun. 11 (1990) 571–576.
[16] K. Nagase, Thermoresponsive interfaces obtained using poly(N-Isopropylacrylamide)-Based copolymer for bioseparation and tissue engineering applications, Adv. Colloid Interface Sci. 295 (2021) 102487.
[17] K. Nagase, M. Yamato, H. Kanazawa, T. Okano, Poly(N-Isopropylacrylamide)-Based thermoresponsive surfaces provide new types of biomedical applications, Biomaterials 153 (2018) 27–48.
[18] T. Ohki, M. Yamato, M. Ota, R. Takagi, D. Murakami, M. Kondo, R. Sasaki, H. Namiki, T. Okano, M. Yamamoto, Prevention of esophageal stricture after endoscopic submucosal dissection using tissue-engineered cell sheets, Gastroenterology 143 (2012) 582–588.e2.
[19] K. Yamamoto, T. Hama, M. Yamato, H. Uchimizu, H. Sugiyama, R. Takagi, Y. Yaguchi, T. Okano, H. Kojima, The effect of transplantation of nasal mucosal epithelial cell sheets after middle ear surgery in a rabbit model, Biomaterials 42 (2015) 87–93.
[20] R. Guo, M. Morimatsu, T. Feng, F. Lan, D. Chang, F. Wan, Y. Ling, Stem cell-derived cell sheet transplantation for heart tissue repair in myocardial infarction, Stem Cell Res. Ther. 11 (2020) 19.

[21] L. Zhou, J. Xia, X. Qiu, P. Wang, R. Jia, Y. Chen, B. Yang, Y. Dai, In vitro evaluation of endothelial progenitor cells from adipose tissue as potential angiogenic cell sources for bladder angiogenesis, PLoS One 10 (2015) e0117644.
[22] L. Zhou, L. Xu, J. Shen, Q. Song, R. Wu, Y. Ge, H. Xin, J. Zhu, J. Wu, R. Jia, Preischemic administration of nonexpanded adipose stromal vascular fraction attenuates acute renal ischemia/reperfusion injury and fibrosis, Stem Cells Transl. Med. 5 (2016) 1277–1288.
[23] L. Zhou, T. Yang, F. Zhao, K. Song, L. Xu, Z. Xu, C. Zhou, Z. Qin, Z. Xu, R. Wu, H. Xu, R. Jia, Effect of uncultured adipose-derived stromal vascular fraction on preventing urethral stricture formation in rats, Sci. Rep. 12 (2022) 3573.
[24] M. Yamato, M. Utsumi, A. Kushida, C. Konno, A. Kikuchi, T. Okano, Thermo-responsive culture dishes allow the intact harvest of multilayered keratinocyte sheets without dispase by reducing temperature, Tissue Eng. 7 (2001) 473–480.
[25] A. Kushida, M. Yamato, C. Konno, A. Kikuchi, Y. Sakurai, T. Okano, Decrease in culture temperature releases monolayer endothelial cell sheets together with deposited Fibronectin matrix from temperature-responsive culture surfaces, J. Biomed. Mater. Res. 45 (1999) 355–362.
[26] M. Yamato, M. Okuhara, F. Karikusa, A. Kikuchi, Y. Sakurai, T. Okano, Signal transduction and cytoskeletal reorganization are required for cell detachment from cell culture surfaces grafted with a temperature-responsive polymer, J. Biomed. Mater. Res. 44 (1999) 44–52.
[27] S. Bou-Ghannam, K. Kim, D.W. Grainger, T. Okano, 3D cell sheet structure augments mesenchymal stem cell cytokine production, Sci. Rep. 11 (2021) 8170.
[28] J.M. Gooding, K.L. Yap, M. Ikura, The cadherin–catenin complex as a focal point of cell adhesion and signalling: new insights from three-dimensional structures, Bioessays 26 (2004) 497–511.
[29] M.-D. Kim, S.-S. Kim, H.-Y. Cha, S.-H. Jang, D.-Y. Chang, W. Kim, H. Suh-Kim, J.-H. Lee, Therapeutic effect of hepatocyte growth factor-secreting mesenchymal stem cells in a rat model of liver fibrosis, Exp. Mol. Med. 46 (2014) e110–e110.
[30] J.S. Choi, D.-S. Chae, H.A. Ryu, S.-W. Kim, Transplantation of human adipose tissue derived-SVF enhance liver function through high anti-inflammatory property, Biochim. Biophys. Acta Mol. Cell Biol. Lipids 1864 (2019) 158526.
[31] B.-S. Kim, S.-H. Chen, M. Vasella, M. Guidi, E. Gousopoulos, N. Lindenblatt, H.-K. Kao, In vivo evaluation of mechanically processed stromal vascular fraction in a chamber vascularized by an arteriovenous shunt, Pharmaceutics 14 (2022) 417.
[32] S. Neuss, E. Becher, M. Wöltje, L. Tietze, W. Jahnen-Dechent, Functional expression of HGF and HGF receptor/C-met in adult human mesenchymal stem cells suggests a role in cell mobilization, tissue repair, and wound healing, Stem Cell. 22 (2004) 405–414.
[33] S. Gharbia, S.-R. Nazarie, S. Dinescu, C. Balta, H. Herman, V.E. Peteu, M. Gherghiceanu, A. Hermenean, M. Costache, Adipose-derived stem cells (ADSCs) supplemented with hepatocyte growth factor (HGF) attenuate hepatic stellate cell activation and liver fibrosis by inhibiting the TGF-β/smad signaling pathway in chemical-induced liver fibrosis associated with diabetes, Cells 11 (2022) 3338.
[34] A.-E. Declèves, K. Sharma, Novel targets of antifibrotic and anti-inflammatory treatment in CKD, Nat. Rev. Nephrol. 10 (2014) 257–267.
[35] B. Al-Sowayan, F. Alammari, A. Alshareeda, Preparing the bone tissue regeneration ground by exosomes: from diagnosis to therapy, Molecules 25 (2020) 4205.
[36] B.S. Cho, J.O. Kim, D.H. Ha, Y.W. Yi, Exosomes derived from human adipose tissue-derived mesenchymal stem cells alleviate atopic dermatitis, Stem Cell Res. Ther. 9 (2018) 187.
[37] M. Zeyda, D. Farmer, J. Todoric, O. Aszmann, M. Speiser, G. Györi, G.J. Zlabinger, T.M. Stulnig, Human adipose tissue macrophages are of an anti-inflammatory phenotype but capable of excessive pro-inflammatory mediator production, Int. J. Obes. 31 (2007) 1420–1428.
[38] D. Karussis, I. Kassis, The potential use of stem cells in multiple sclerosis: an overview of the preclinical experience, Clin. Neurol. Neurosurg. 110 (2008) 889–896.
[39] H.D. Zomer, T.D.S. Jeremias, B. Ratner, A.G. Trentin, Mesenchymal stromal cells from dermal and adipose tissues induce macrophage polarization to a pro-repair phenotype and improve skin wound healing, Cytotherapy 22 (2020) 247–260.